PROCEEDINGS, 51st Workshop on Geothermal Reservoir Engineering
Stanford University, Stanford, California, February 9-11, 2026
SGP-TR-230

Characterization of Mineral Scales and Corrosion Products at the Utah FORGE Enhanced Geothermal System Laboratory

Clay G. Jones, Stuart F. Simmons and Joseph N. Moore

Energy & Geoscience Institute at the University of Utah 155 S 1452 E, rm 222, Salt Lake City, UT 84112

cjones@egi.utah.edu

Keywords: Mineral Scale, Corrosion, Fluid Chemistry, Fluid Additives, EGS, SEM, XRD, EDS, XRF

ABSTRACT

Repeated stimulation, circulation, and cleanout operations at Utah FORGE have produced a suite of solid mineral scales and corrosion products recovered from the subsurface and surface infrastructure. This study synthesizes mineralogical and textural observations from these scale and corrosion samples collected between 2019 and 2025. These observations are then related to mineral saturation perturbations due to cyclic temperature and composition changes during circulation activities. In addition, we document effective fluid additives for scale and corrosion mitigation used to date at Utah FORGE, and those proposed for future, longer term circulation testing. Scale and corrosion products were characterized by using X-ray diffraction, a scanning electron microscope equipped with an energy-dispersive spectroscopy, and X-ray fluorescence. Mineral scales consist of calcite, siderite, anhydrite, halite, sylvite, and a Fe- and Si-rich expandable smectite group clay. Corrosion products include magnetite, hematite, lepidocrocite, and goethite, as well as boehmite and an Al-bearing phase with structural similarity with greenalite, reflecting both iron and aluminum infrastructure degradation, respectively. Carbonates and anhydrite are expected to deposit from injection waters on heating in the wellbore and/or within the fracture network in the reservoir rocks. Incorporation of CO_2 into the fluids in the reservoir lowers pH and somewhat inhibits carbonate deposition. Rapid equilibration with quartz in the reservoir results in the potential for silica scaling on cooling in the production wellbore and topside equipment. After significant scaling issues were encountered in 2024 during stimulation activities, a scale and corrosion mitigation strategy was employed by dosing the injected fluids with additives that has been effective during subsequent cleanout and circulation activities.1.

1. INTRODUCTION

The Utah Frontier Observatory for Research in Geothermal Energy (FORGE) is a US Department of Energy funded underground field laboratory in southwest Utah for developing, testing, and accelerating breakthroughs in Enhanced Geothermal Systems (EGS) technologies.

This study presents a multi-year mineralogical investigation of scale and corrosion products recovered from subsurface and surface infrastructure at Utah FORGE. Samples were collected between 2019 and 2025 (Figure 1). Scale and corrosion samples from the subsurface come from packers, geophones, drill pipe, proppants, bottom hole assemblies, and groundwater well tubing. A surface sample comes from a steam-brine separator. The scale and corrosion products were analyzed for textural information using a scanning electron microscope, X-ray diffraction was used to investigate crystalline structures and quantify abundances is polymineralic samples, and elemental compositions were determined via energy-dispersive spectroscopy and X-ray fluorescence.

Mineral deposition commonly occurs in wells, reservoir rocks and surface equipment of hydrothermal systems in response to temperature, pressure and chemical perturbations during injection and production. EGS systems offer additional layers of complication due to: short fluid residence times in the fractured reservoir rock; pronounced cyclic fluid pressure-temperature changes; rapid compositional changes within the reservoir; and fluid mixing (e.g. adding makeup water).

EGS systems require significant upfront investment before revenue is generated, from well drilling, to stimulation, to constructing power generation infrastructure. Mineral scaling and corrosion have the potential to reduce permeability and decrease heat sweep efficiency in the fractured reservoir rocks, and to degrade well and topside infrastructure. Mitigating these risks requires: frequent geochemical data collection; an understanding of the impact of evolving P-T conditions on mineral saturation indices; characterization of solid mineral scale and corrosion products; and implementing a fluid additive program to inhibit scale and corrosion.

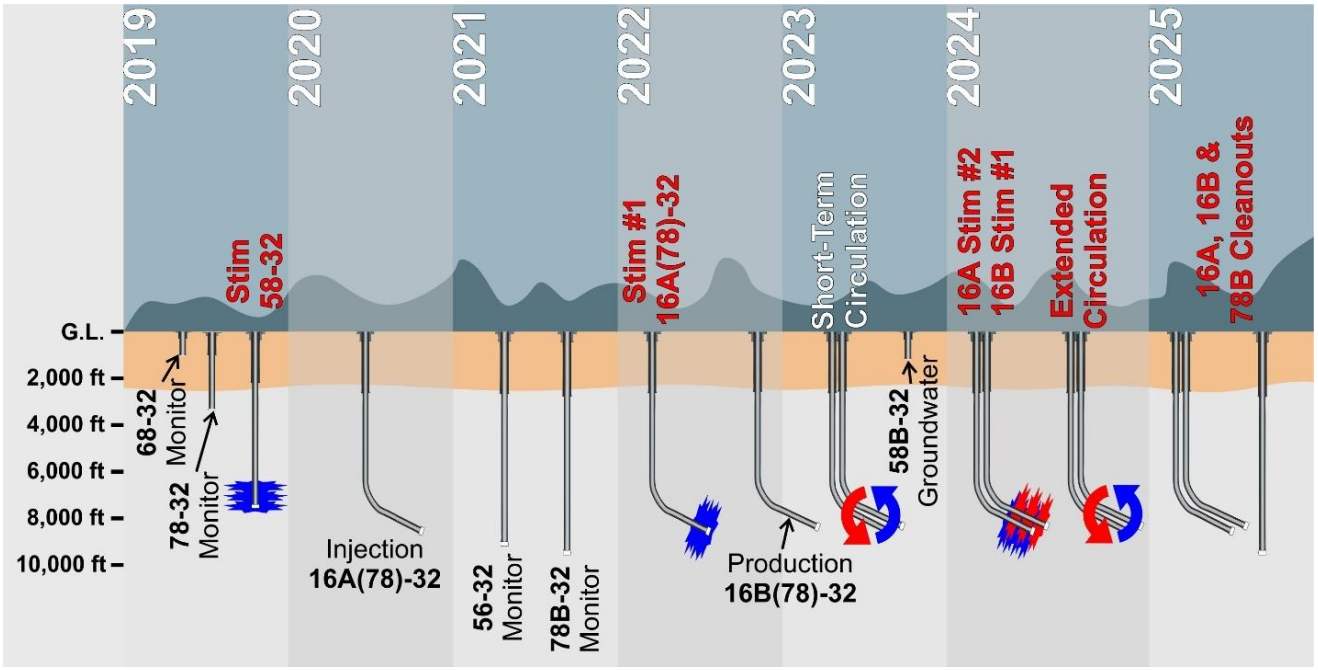

Figure 1. Schematic summary of Utah FORGE activities vs time from 2019 through 2025, with red labels indicating events when scale and corrosion products that were observed and collected.

2. ANALYTICAL METHODS FOR CHARACTERIZATION

2.1. X-Ray diffraction (XRD)

XRD data was obtained using a Bruker D8 Advance X-ray diffractometer at the Energy & Geoscience Institute at the University of Utah. Whole rock, powdered samples were analyzed to determine crystalline phase abundances. Oriented clay-sized (< 5 μm) slurry mount samples were prepared for air-dried and glycolated state data acquisition to assess the expandability and determine the structures of clay minerals.

2.2. Scanning electron microscope (SEM), back-scatter electron (BSE) imaging and energy dispersive spectroscopy (EDS)

A JEOL IT-300 SEM equipped with an Oxford X-act EDS detector at the Energy & Geoscience Institute at the University of Utah was used to collect BSE images and elemental EDS data from the scale and corrosion samples.

2.3. X-Ray florescence (XRF)

An Olympus Vanta M-series handheld XRF analyzer at the Utah Geological Survey was used to collect elemental data.

3. CHARACTERIZATION OF MINERAL SCALES AND CORROSION PRODUCTS

3.1. 2019- Failed Packer in Well 58-32

Thin (~1 mm) wafer-like solids intermixed with a black, tar-like substance were recovered from a failed packer. The wafers exhibit distinct color zonation, with one surface being dark reddish-brown, a gray interior, and an opposing lighter tan-orange surface (Figure 2). XRD analysis identified quartz, calcite, calcium aluminoferrite, portlandite, and siderite as mineral components. Quartz, calcium aluminoferrite, and portlandite come from the gray cement in the interior for the wafers. Subhedral siderite occurs on the darker surface that is interpreted to have formed adjacent to the steel well casing. Complex euhedral calcite crystals occur on the lighter surface and are interpreted to have grown into open space. The black tar-like substance is likely thermally degraded elastomer from the expandable elements of the packer.

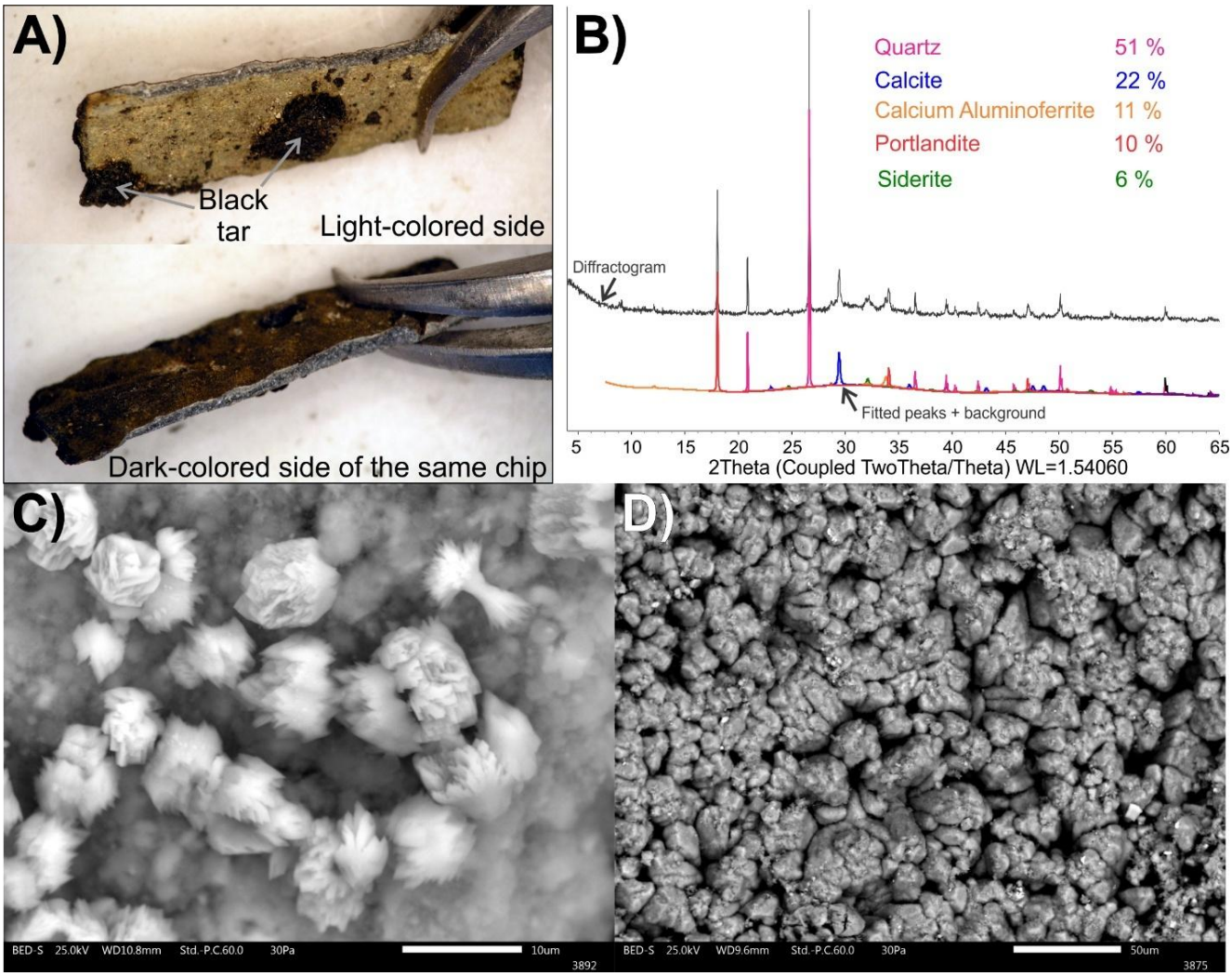

Figure 2. Binocular microscope and SEM-BSE images of the thin (~1 mm) wafer-like scale fragments recovered from a failed packer in well 58-32 in 2019, as well as XRD data. A) The wafers show distinct color zonation, with a dark reddish-brown surface, a gray interior, and a lighter tan-orange surface. The darker surface is dominated by siderite and is interpreted to have been adjacent to the steel well casing. The gray center is a thin film of cement consisting of quartz, calcium aluminoferrite, and portlandite. The lighter-colored side is coated by complex euhedral calcite crystals and is interpreted to have formed in open space in the interior of the casing. B) Bulk XRD data with phase abundances in weight percent, the measured diffractogram and the calculated pattern consisting of peaks and background. C) SEM-BSE image of complex euhedral calcite crystals growing into the pipe interior on the lighter colored surface. D) SEM-BSE image of subhedral siderite crystals forming on the surface adjacent to the steel casing.

3.2. 2022 Geophone Corrosion

Geophones deployed in vertical monitoring wells 58-32 and 78B-32 in late September 2022 experienced rapid degradation within a few days and were retrieved in January 2023. The geophones were deployed to monitor microseismic activity during the stimulation of well 16A(78)-32. These geophones were deployed in well 58-32 between 5,000 and 6,000 ft measured depth where temperatures ranged from 150 to 170°C, and between 6,000 and 7,000 ft at temperatures from 170 to 190°C in well 78B-32. White corrosion products were observed aluminum components with comparably little corrosion observed on the steel components (Figure 3). XRD and SEM-EDS analyses indicate that these products consist primarily of boehmite (AlO(OH); 85–97 wt%), with a later Fe- Al- and Si-bearing phase with a structure resembling greenalite ($Fe_3Si_2O_5(OH)_4$), likely with Al for Fe and/or Si substitution as suggested by the imperfect match to XRD reference patterns. SEM analyses shows that boehmite precipitated prior to the Al-rich greenalite-like phase.

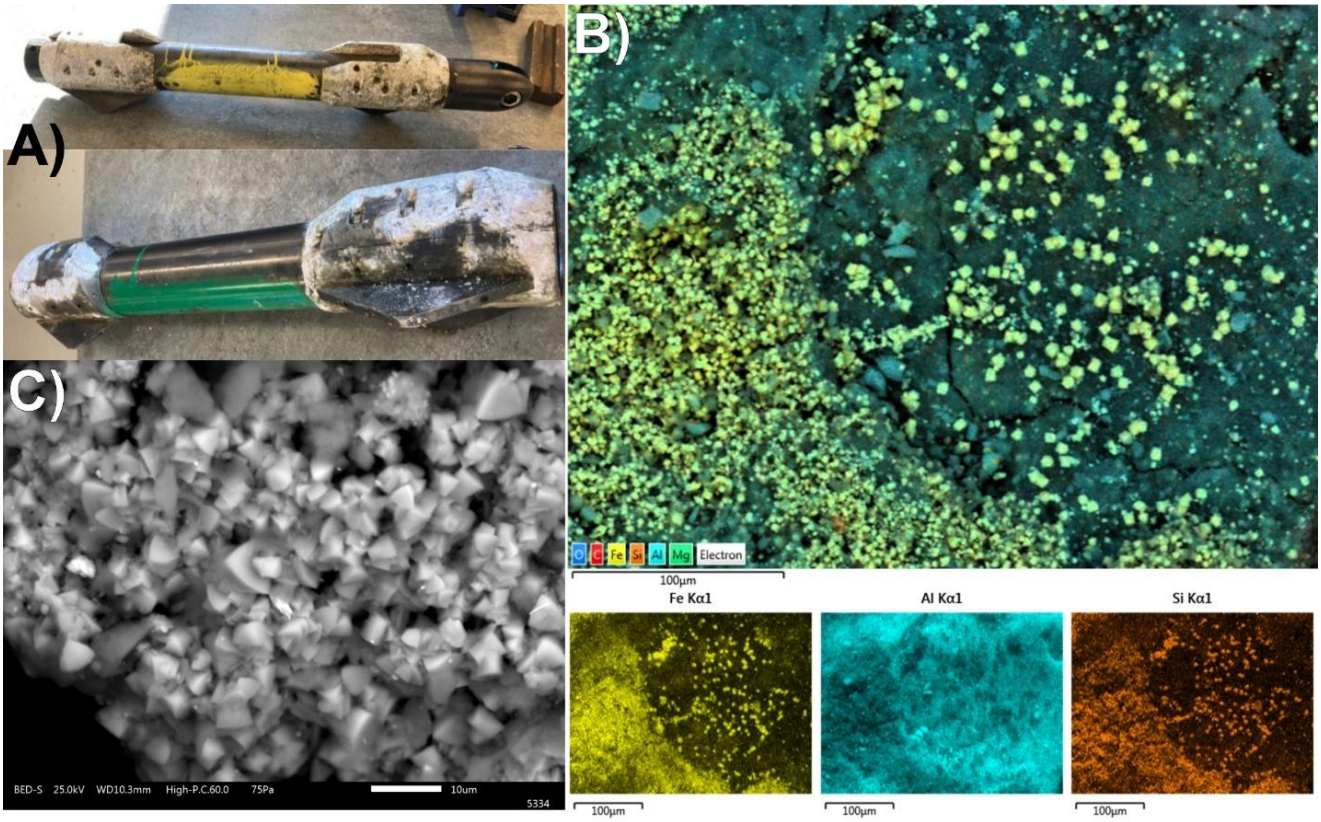

Figure 3. Images of white corrosion products observed on aluminum components of geophones deployed in wells 58-32 and 78B-32, as well as SEM-EDS maps. A) images of the recovered geophones with white corrosion products on the Al components. B) SEM-EDS maps showing small equant crystals of the Al-rich greenalite-like phase on a subsurface of boehmite. The larger image is a composite map, with maps of the same extent for selected individual elements presented below. C) SEM-BSE image of euhedral, equant crystals of the greenalite-like phase.

3.3. 2024 16A & 16B Stimulation and Extended Circulation Test Scales

Scale samples from drill pipe (Figure 4) and a frac plug that formed in the subsurface during the stimulation of injection well 16A(78)-32 and production well 16B(78)-32 are dominated by calcite, with variable morphologies, accompanied by magnetite. Quartz is only observed in scale samples from 16B, both quartz sand and C-rich ultra-lightweight proppant transported from a stimulation stage in16A through the fractures in the EGS reservoir were observed during SEM investigations. It was during this period that significant scaling issues were first noted, establishing the need for improved water treatment to mitigate scaling and corrosion during operations. From this point on all injected fluids were treated to mitigate scaling and corrosion (see Section 5 for more details on scaling and corrosion mitigation).

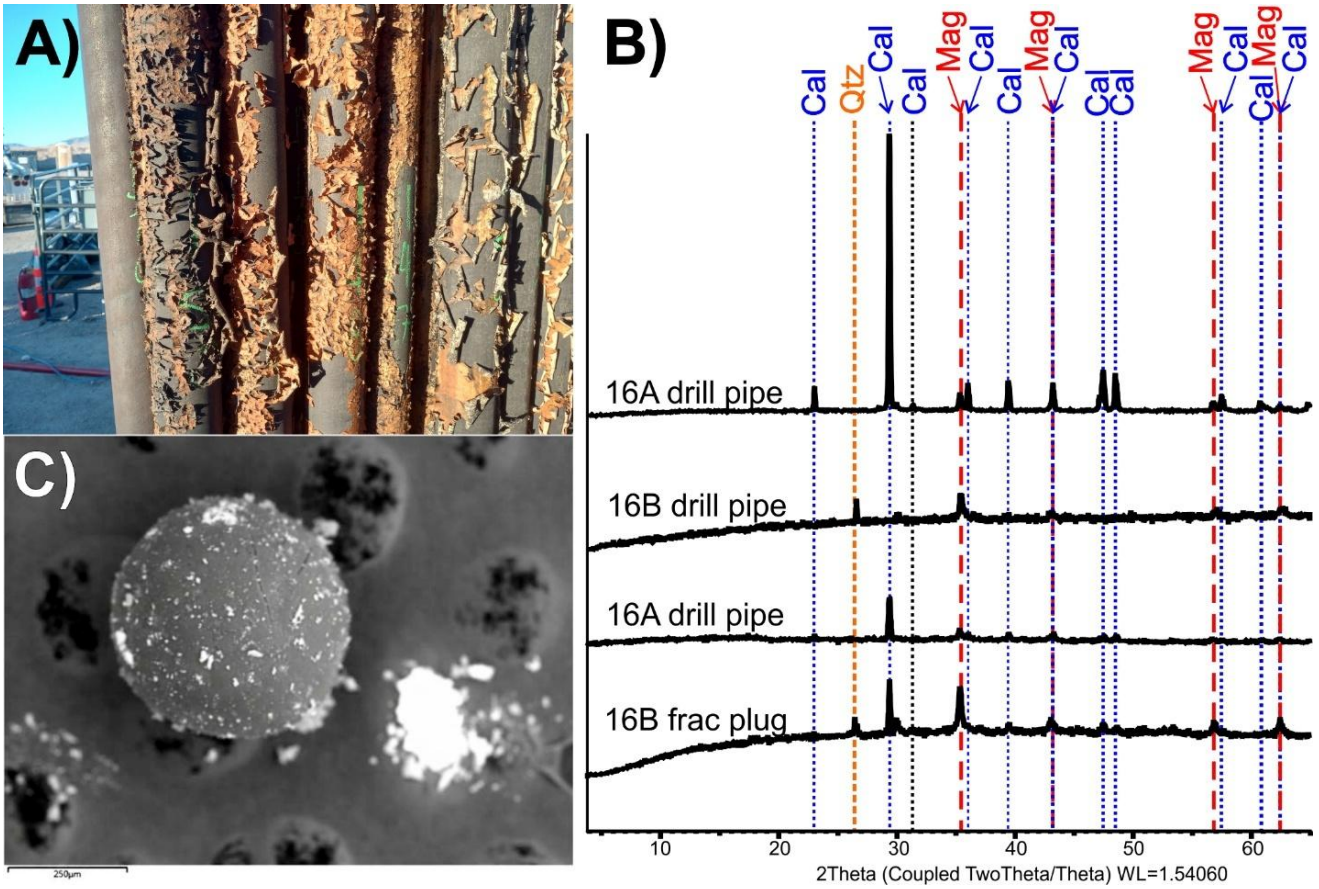

Figure 4. images of scale samples on drill pipe, proppants within scale samples and XRD data from scales. A) image of bark-like scale that developed on drill pipe deployed in the wells. B) XRD diffractograms from four scale samples with peak locations for calcite (Cal), magnetite (Mag) and quartz (Qtz) annotated. C) SEM-BSE image of an ultra-light weight proppant on carbon tape.

The recovered 'sludge' from the extended circulation test between 16A and 16B, that followed stimulation, consisted of dark oily material containing rubbery sheets and thin solid flakes. The solid flakes were extracted from the 'sludge' for analyses by first rinsing with deionized water, then with acetone in combination with an ultrasonic bath. The flakes exhibit two distinct surfaces (Figure 5): 1) a porous magnetite, and 2) calcite with variable morphology partially coated by fine-grained magnetite. XRD diffractograms are similar to the pipe and packer scales from the earlier stimulation of 16A and 16B, with calcite dominating (69 wt%), less abundant magnetite (30 wt%) and minor lead (1 wt%). Lead was also observed in during SEM analyses and is interpreted to be a contaminant from 'pipe dope'. The porous magnetite side is interpreted to have formed against iron components (drill pipe, casing and/or frac plugs), and the calcite before magnetite side growing into open space. SEM observations demonstrate early calcite precipitation followed by magnetite during later stages of scale development. A set of unwashed dried and powdered 'sludge' samples were analyzed by XRF at the Utah Geological Survey, showing that they contain significant Ca (23 wt%) and Fe (16 wt%), consistent with calcite and magnetite.

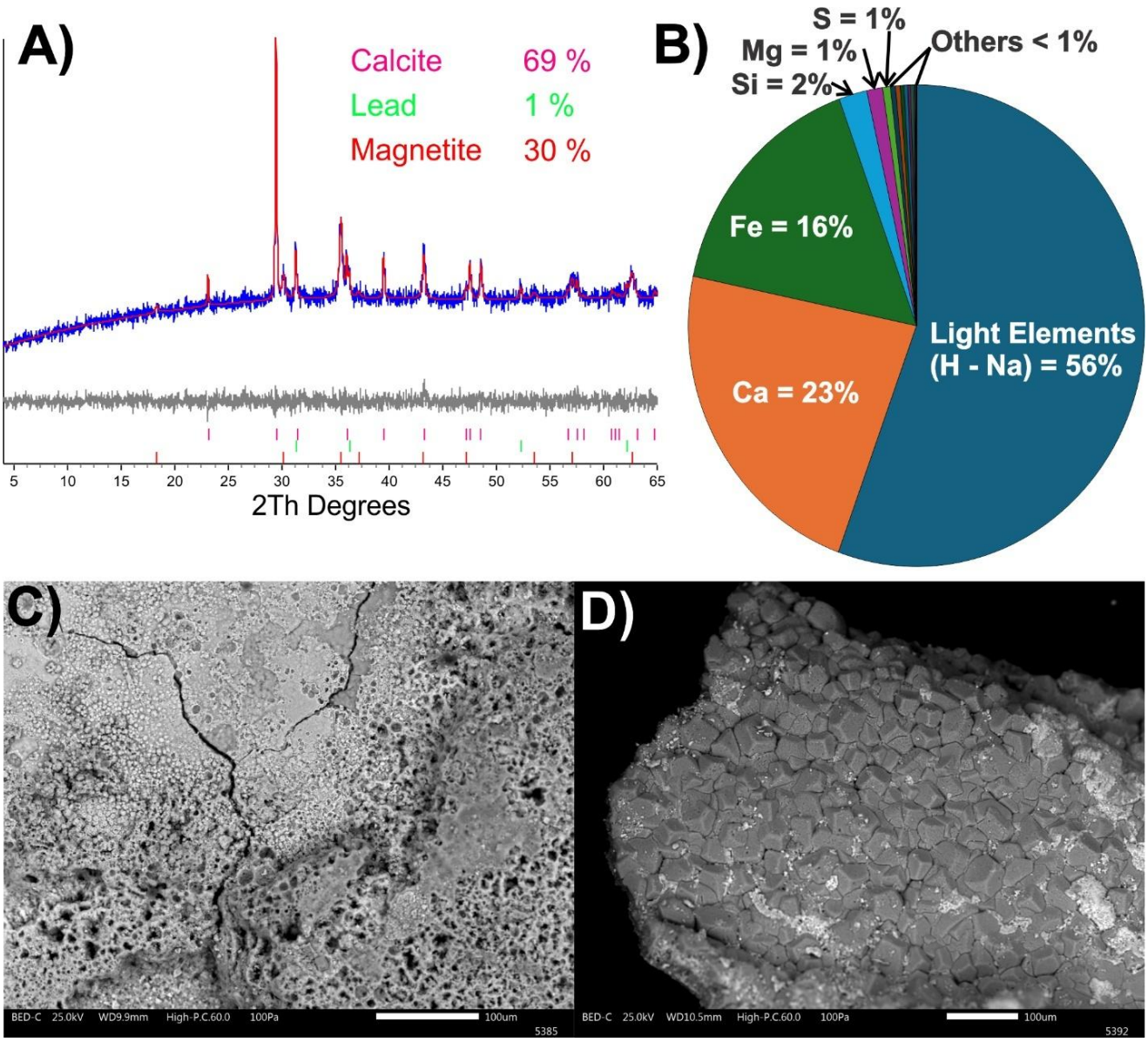

Figure 5. XRD, XRF and SEM analyses of the 'sludge' recovered during the extended circulation test between injector 16A and producer 16B in 2024. A) XRD diffractogram (blue), calculated pattern match (red) difference (gray) and results in wt % of sample. B) Results of XRF analyses performed at the UGS. C) SEM-BSE image of the porous, magnetite rich side of the scale chips, interpreted have formed adjacent to iron infrastructure. D) A SEM-BSE image of the euhedral calcite partially coated by lighter colored magnate interpreted to be growing into open space.

3.4. 2025 Proppants Recovered from Well 16A(78)-32

During cleanout operations of injection well 16A in 2025 four samples of quartz sand proppant were recovered that infilled the wellbore below the stage 3 perforations (Figure 6). These samples were recovered from depths of 10,360, 10,630, 10,700 and 10,775 ft measured depth. The proppants were submerged in the wellbore for approximately 14 months, having been injected during stimulation activities in April 2024, and recovered in June 2025. These analyses demonstrate dissolution of the proppant sand, and the precipitation of secondary mineral phases within the proppant filled wellbore.

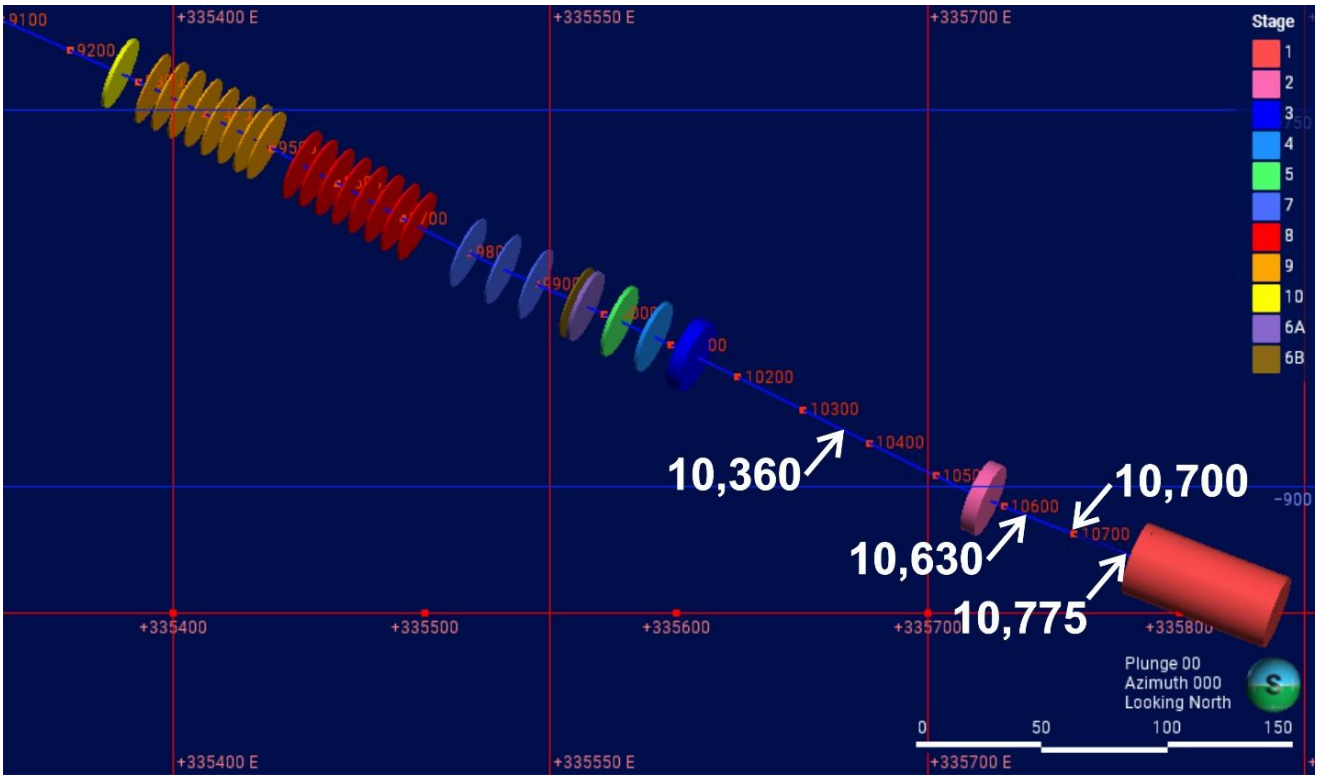

Figure 6: A view of the Leapfrog Energy 3D model of the Utah FORGE site showing the trajectory of injection well 16A(78)-32 with open hole and perforated intervals shown as large diameter discs color coded to stage as shown in the legend. The depths from which proppant were recovered are annotated in white.

Dissolution textures were observed in the proppants during SEM analyses, made readily apparent by comparison to the texture of sand grains from a batch of unused proppants (Figure 7). Feldspar grains, a minor component of the proppant sand are more prone to dissolution than quartz grains. Dissolution textures were the least pronounced in the deepest sample from 10,775 ft.

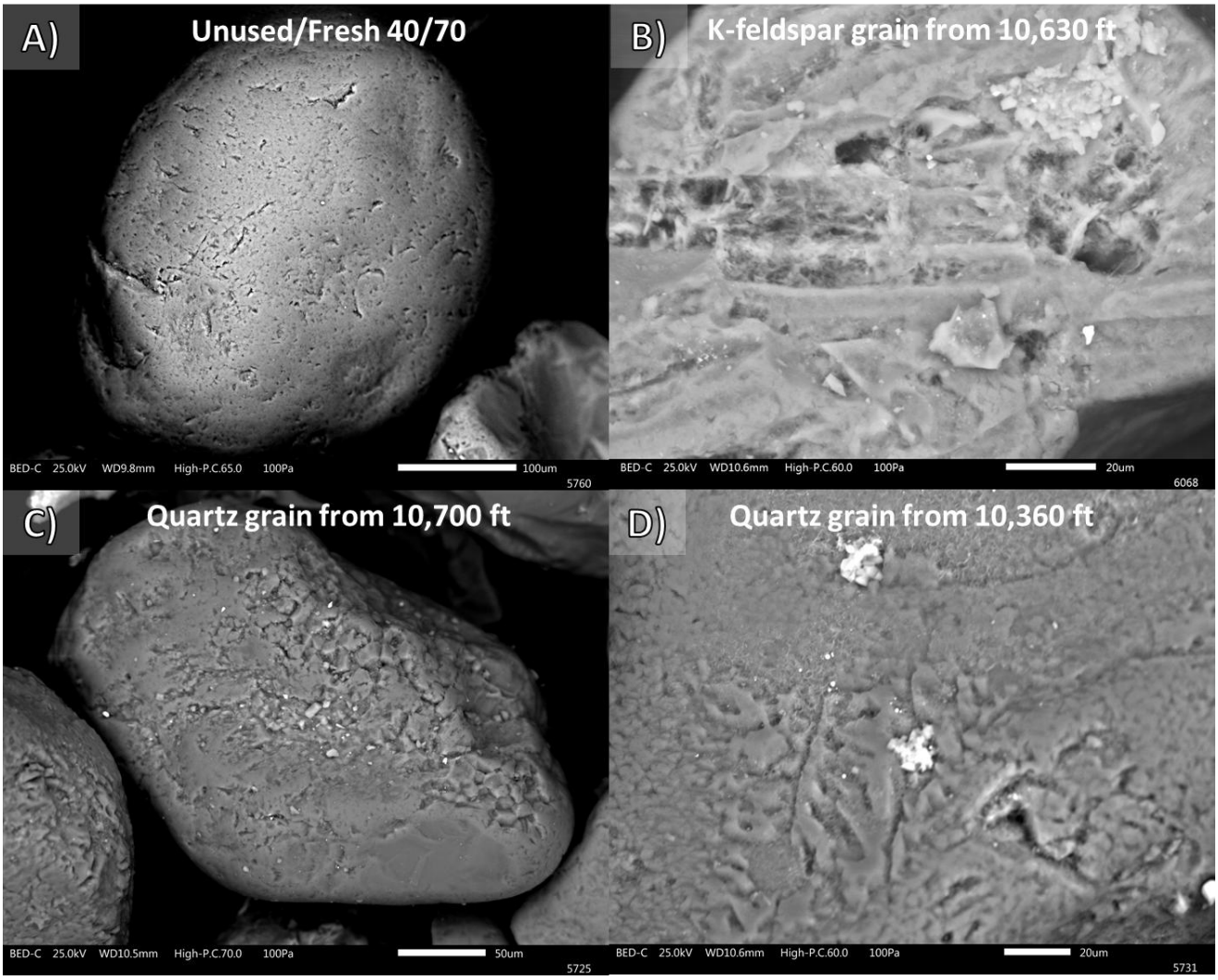

Figure 7: SEM-BSE images comparing surface textures of unused, 'fresh' quartz proppant (A) in comparison to K-feldspar (B) and quartz (C&D) proppants that had remained in the 16A wellbore for ~14 months. Dissolution textures are more pronounced in K-feldspar grains (B) than in quartz (C&D). Dissolution textures indicate the active mobilization of silica and other elements in the wellbore.

Coating of clay minerals on the surface of the proppants was most common in the uppermost sample from 10,360 ft and diminishes in both abundance and thickness with depth. Clay mineral coatings range from a thin, furry film, up to at least 5 µm thick (Figure 8). SEM-EDS data collected from the thickest observed occurrence of the clay shows that it is composed dominantly of Fe and Si with lesser Al, Mg, Na, Cl, K and Ca. To investigate the structure of the clay mineral, an aliquot of the proppant sand sample from 10,360 ft was mechanically agitated to remove the clay coatings and analyzed by XRD in an oriented slurry mount. The sample was scanned after air drying, and again after interacting with ethylene glycol vapors for > 24 hrs. A comparison of the two scans (Figure 11) shows shifts characteristic of an expandable clay of the smectite group (Moore and Reynolds, 1997).

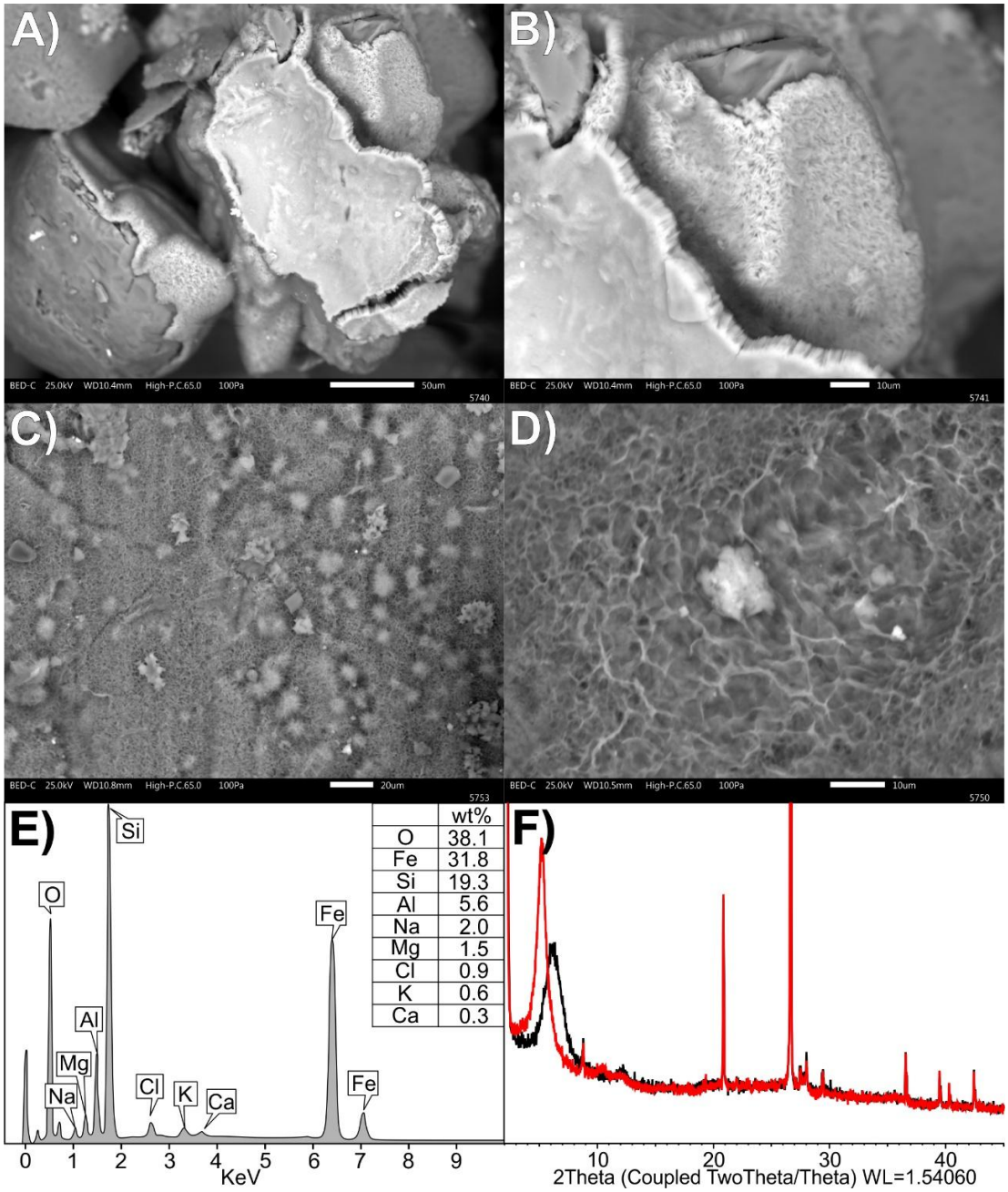

Figure 8: SEM-BSE images of the expandable, Fe and Si-rich, clay mineral coating proppant grains from the sample recovered from 10,360 ft measured depth in injection well 16A(78)-32 as well as SEM-EDS and XRD data acquired from the clay mineral. A&B) are SEM-BSE images of the thickest observed occurrence at ~5 µm. C&D) are SEM-BSE images of more typical thin, fury films coating proppant grains. E) SEM-EDS spectra obtained from the area annotated in panel B. F) Diffractograms of an oriented mount of fine-grained material separated from sample 10,360 ft after mechanical agitation. The magnitude of the shift observed between the air-dried (black) and glycolated (red) peaks at low 2Theta is characteristic of expandable clays of the smectite group (Moore and Reynolds, 1997).

Salts were observed coating proppants in all samples (Figure 9). Halite is the dominant species with minor sylvite. Salts in the shallowest sample at 10,360 ft were finer-grained with anhedral textures that are interpreted to represent partial dissolution. Salt crystals become coarser-grained below with abundances highest in the intermediate samples from 10,630 and 10,700 ft, with relatively few examples observed in the deepest sample from 10,775 ft.

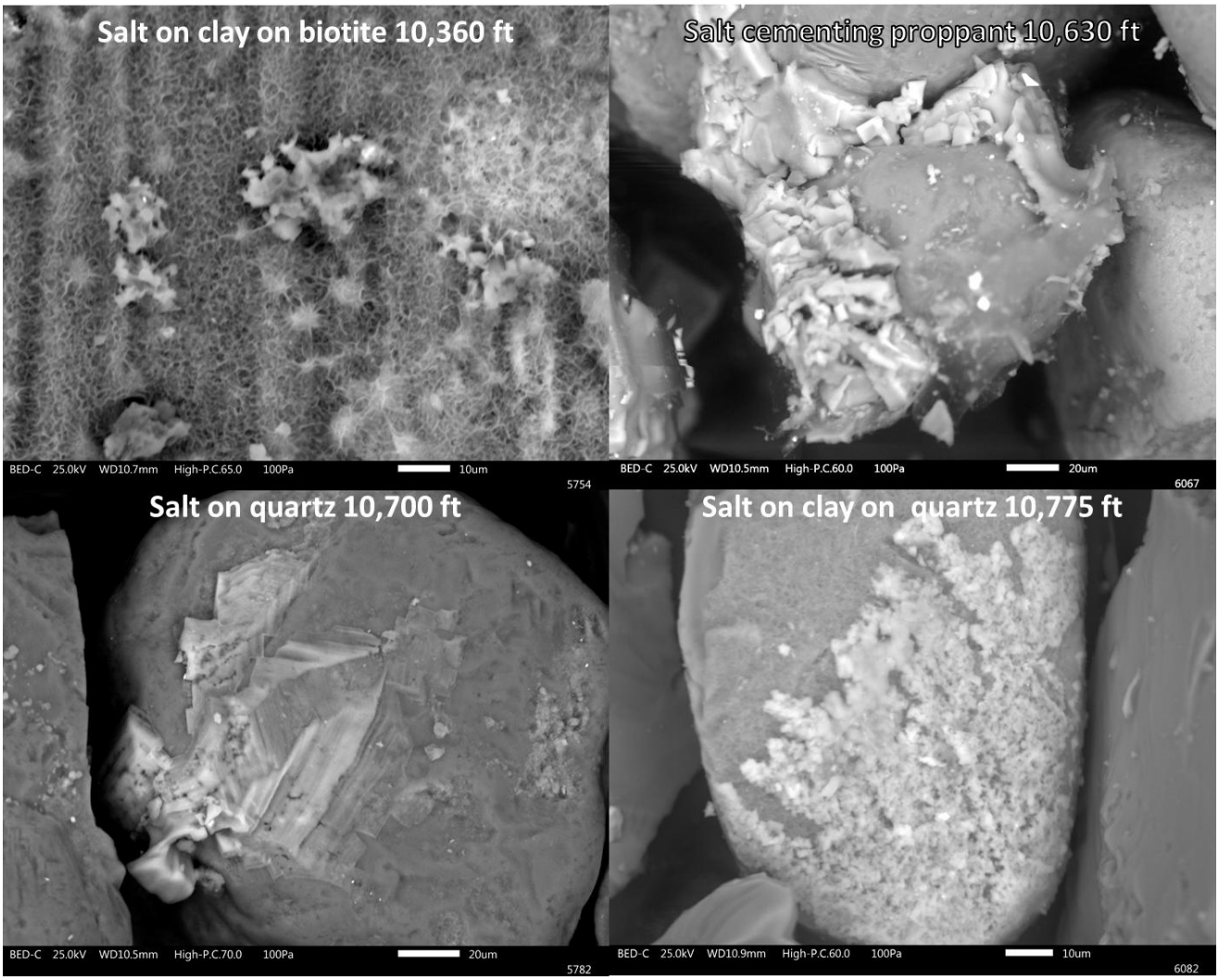

Figure 9: EM-BSE images of halite and minor sylvite (lighter gray) precipitated on recovered proppants from the depths indicated in annotations. Finer, anhedral salt textures at 10,360 ft suggest more active dissolution, whereas coarser, euhedral salts at greater depth indicate more stable precipitation conditions.

Calcite, anhydrite and barite are rare phases observed in all samples (Figure 10). Anhydrite can have an unusual morphology with embayments that are interpreted to be the result of partial dissolution (Figure 10C). Anhydrite formation is assumed to be in-situ, and subsequent dissolution suggests oscillating P-T-X conditions. The low abundances of calcite and anhydrite are consistent with effective scale inhibitor performance. Anhydrite and calcite are expected to form on heating (see Section 4) and to precipitate from injected fluids in the deepest hottest parts of the 16A wellbore. At least locally, halite precipitates prior to calcite (Figure 11).

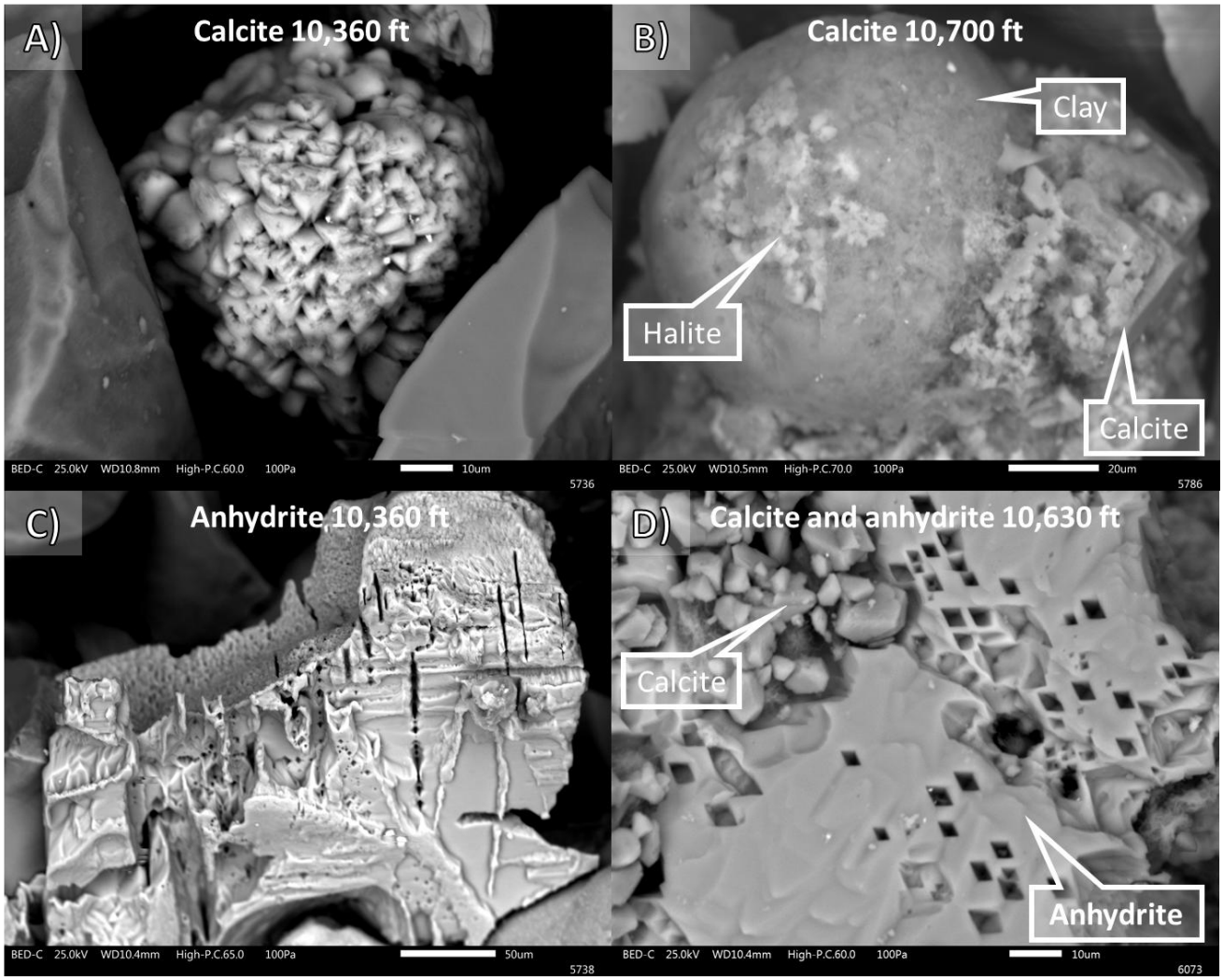

Figure 10: SEM-BSE images of calcite and anhydrite observed with samples of recovered proppant form injection well 16A(78)-32 after remaining in the well bore for ~14 months. Localized dissolution textures in anhydrite (C) suggest oscillating P-T-X conditions.

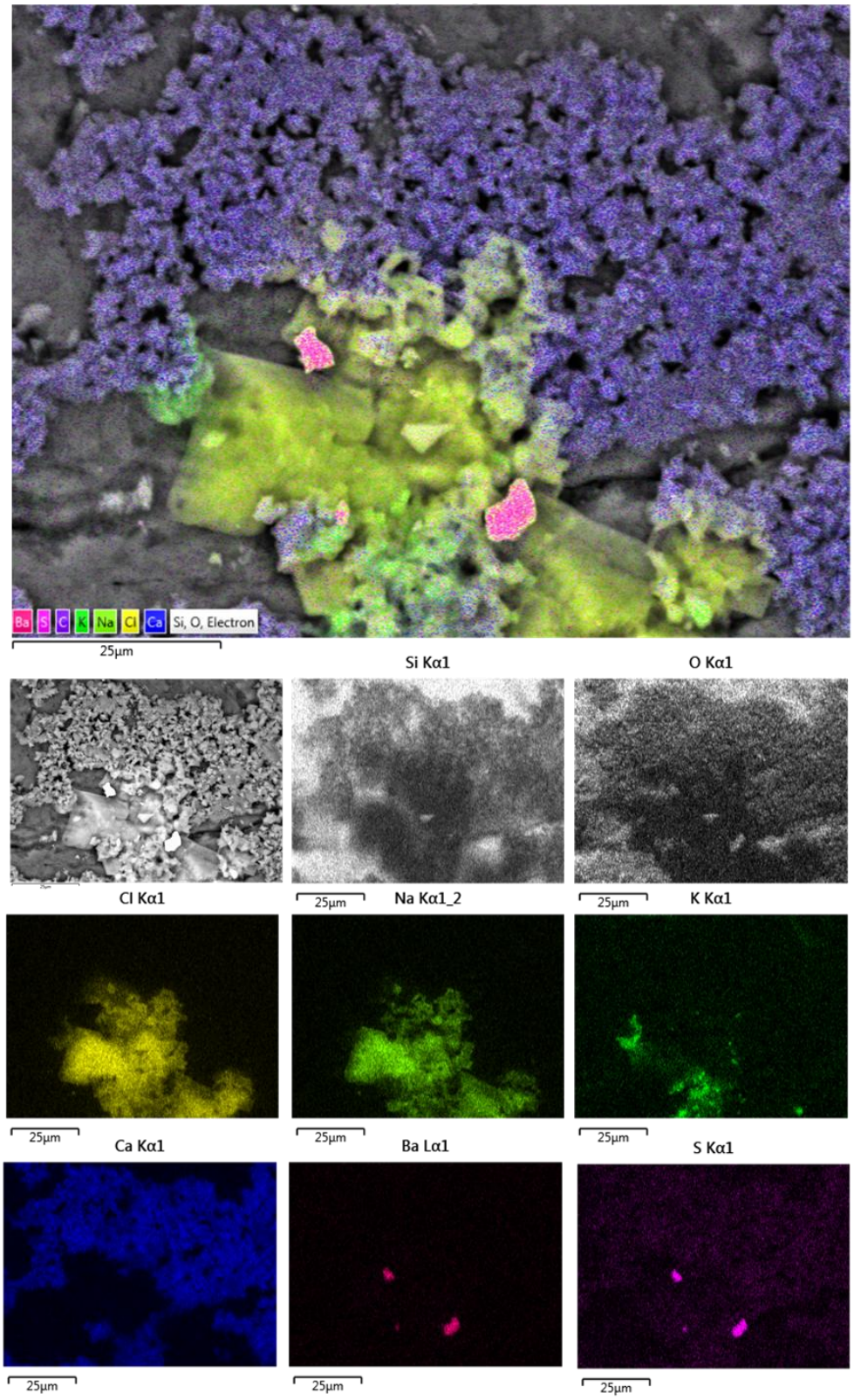

Figure 11: At top is a SEM-BSE image overlain by a composite SEM-EDS elemental map color coded by element as shown at bottom left. The SEM-BSE image is the top-left thumbnail below the composite EDS map. The other smaller images are individual elemental maps showing distribution and abundances. These images show early salt deposition, covered by later calcite on a quartz sand proppant grain.

3.5. 2025 Plugged BHA in 78B-32 and Additional Corrosion Products from Groundwater well 58B-32

XRD analyses (Figure 12) from a plugged bottom hole assemblies (BHA) in well 78B-32 during cleanout operations shows material recovered consists primarily of calcite (86 to 37 wt%), with minor quartz (28.4 to 7 wt%), magnetite (18 to 4 wt%), and hematite (14 to 3 wt%). Calcite is likely a scale product and magnetite and hematite are likely corrosion products. With only XRD data from this sample the origin of quartz is unclear. Proppant has not been introduced into this offset, vertical monitoring well.

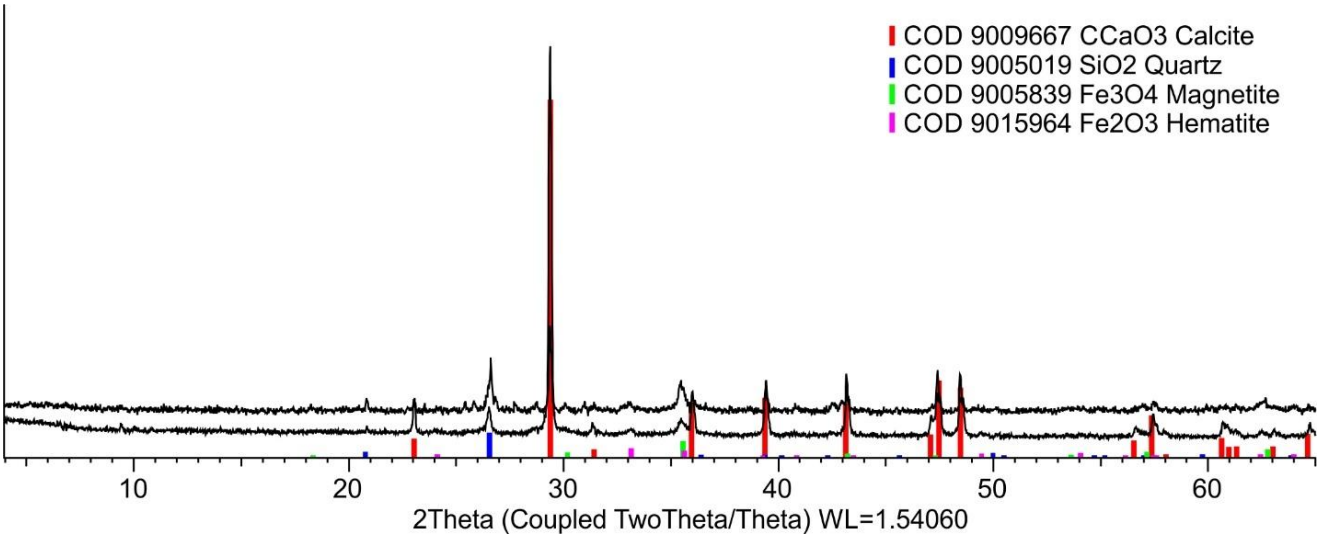

Figure 12: X-ray diffractograms from two samples recovered from plugged bottom hole assemblies during remediation operations in well 78B-32 in 2025. Vertical, color-coded lines are Crystallography Open Database (COD) references for peak locations and intensities for calcite, quartz, magnetite and hematite.

3.6. 2025 Corrosion Products from Groundwater Well 58B-32

A mechanical failure of the pump and motor in groundwater well 58B-32 required the tubing to be removed from the wellbore in 2025. The steel tubing was found to be highly corroded, especially near the water line (Figure 13). XRD analyses shows the corrosion products of the steel tubing consist of magnetite (63 wt%), hematite (13 wt%), goethite (13 wt%) and lepidocrocite (11 wt%).

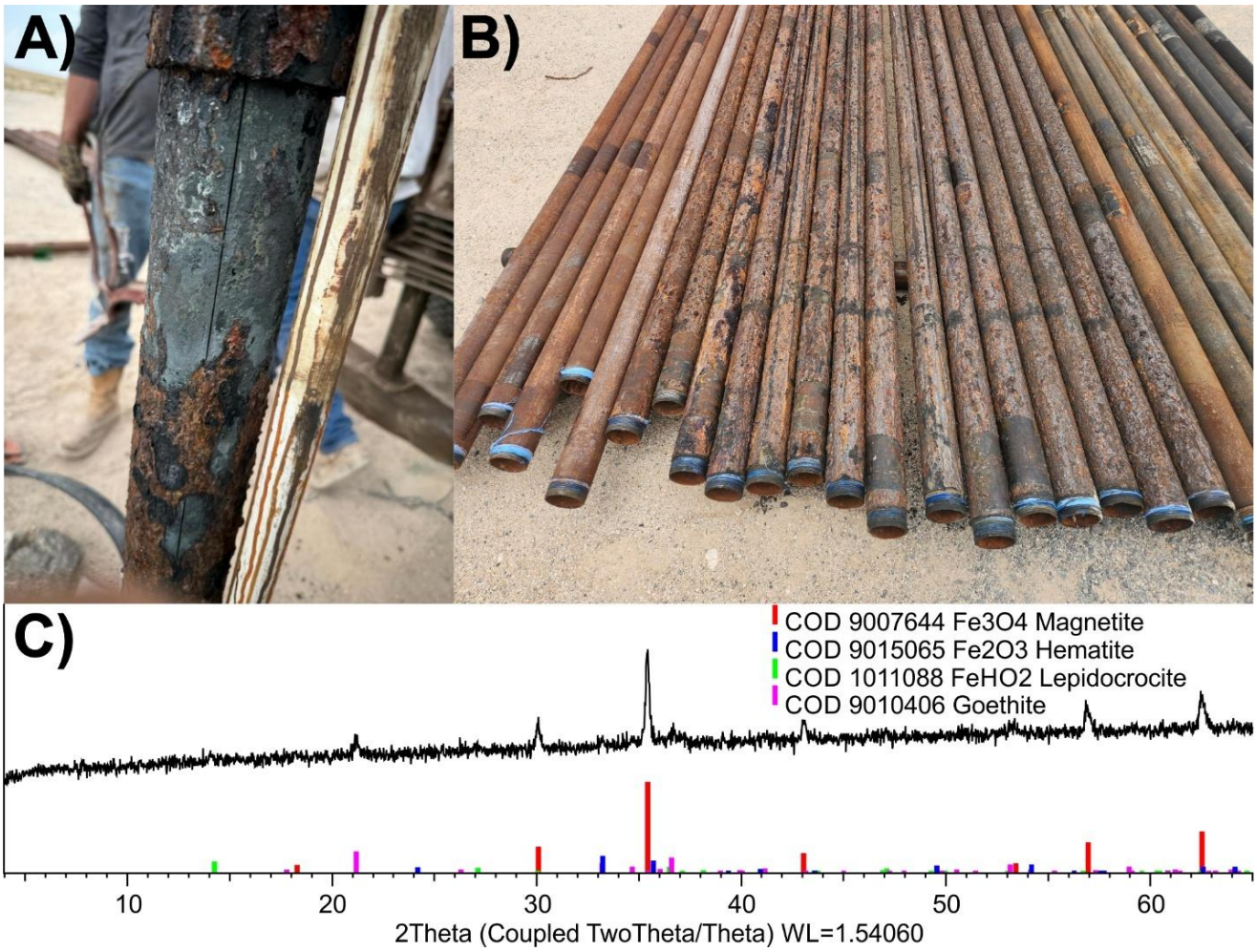

Figure 13. Images of the tubing pulled from groundwater well 58B-32 showing significant corrosion (A&B). X-ray diffractogram of the sampled corrosion product with vertical, color-coded lines indicating peak locations and intensities from reference patterns from the Crystallography Open Database (COD) for magnetite, hematite, lepidocrocite and goethite.

3.7. 2025 Separator scale

A steam-brine separator (Figure 14) that had seen use from 2022 onwards was cleaned out in 2025. The interior of the separator constrained significant scale that had accumulated during flow back operations after stimulations and circulation testing. XRD analyses shows that the scale consisted dominantly of calcite (98 wt%), with minor quartz (2 wt%, likely produced proppant), consistent with mineral precipitation expected during rapid P-T-X changes associated with fluid flashing.

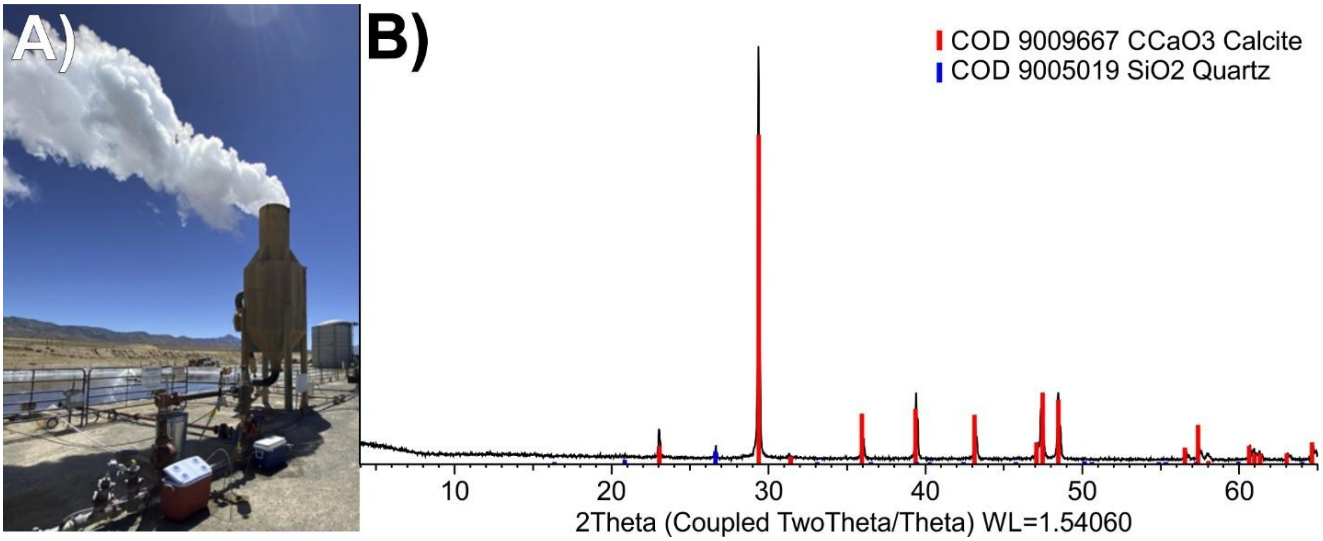

Figure 14: A) An image of the separator with steam exiting the top during a circulation experiment. B) X-ray diffractogram of the scale collected from the interior of the separator after cleanout, with vertical, color-coded lines indicating peak locations and intensities from reference patterns from the Crystallography Open Database (COD) for calcite and quartz.

3.8. Summary of Scale and Corrosion Products

Across all samples, calcite is the most commonly observed scale mineral, accompanied by minor siderite, anhydrite, halite, sylvite, and an expandable Fe-rich clay mineral. Corrosion products vary by substrate, with iron-bearing components forming magnetite, hematite, lepidocrocite, and goethite; whereas boehmite and an Al-rich greenalite-like phase are observed on aluminum components.

Table 1: Summary table of scale and corrosion products observed at the Utah FORGE site by location and date. Samples with well names listed under location come from the subsurface.

Location	Description	Date	Scale/Corrosion Phases
58-32	Failed Packer	2019	Calcite & siderite
58-32 78B-32	Corroded Geophones	2022	Boehmite & an Al-rich greenalite-like phase
16A(78)-32 16B(78)-32	Drill Pipe, Frac Plug & Sludge	2024	Calcite & magnetite
16A(78)-32	Proppant	2025	Calcite, smectite group expendable clay, halite, sylvite, anhydrite & barite
78B-32	Plugged BHA	2025	Calcite, quartz(?), magnetite & hematite
58B-32	Pipe Corrosion	2025	Magnetite, hematite, goethite & lepidocrocite
Separator	Clean Out	2025	Calcite & quartz(?)

4. ANALYSES OF MINERAL SATURATION IN INJECTED AND PRODUCED FLUIDS

Although the Utah FORGE EGS reservoir is within relatively nonreactive hot dry alumino-silicate rich rocks (Jones et al., 2024), significant changes in fluid chemistry have been observed after interaction with reservoir rocks over short time scales during stimulation and circulation activities (Jones et al., 2023; Simmons et al., 2025). This is attributed to: soluble salts; carbonates and sulfates that line pre-existing fractures; the presence of quartz in the reservoir rocks, and as proppant placed within stimulated fractures; and infiltration of deep sourced carbon dioxide into the injected fluids. During circulation testing fluids will undergo multiple cycles of heating and cooling from 65 °C and 1.4 MPa at the surface to >200 °C and 48 MPa in the reservoir, with residence times as short as a few hours. The injectate is a near neutral pH, chloride dominant water that contains significant calcium and magnesium (Simmons et al., 2025).

In Figure 15 the computed saturation indices and pH of fluids injected into well 16A(78)-32 (on the left-hand side) and fluids produced from well 16B(78)-32 (on the right-hand side) are shown at temperatures expected during circulation. The plotted values are based on geochemical analyses of waters injected and produced during a circulation test on September 3, 2024 (Simmons et al., 2025). Saturation indices and pH were determined using the Spec8 module in Geochemists Workbench to provide a first-order understanding of the thermal conditions where secondary phases are likely to dissolve or precipitate. Values above zero represent supersaturated waters, and values below zero represent undersaturated waters. The calculations assume thermodynamic equilibria with kinetic effects being ignored.

On the left-hand side of Figure 15, as fluids are heated on injection, carbonate minerals are prone to deposition in the wellbore and in the fracture network of the EGS reservoir at temperatures >~60°C. On the right-hand side, as fluids are cooled on production, quartz and amorphous silica are prone to deposition in surface pipework and equipment. As the fluid traverses the hot reservoir, aqueous silica attains a maximum concentration of ~300 ppm, indicating equilibration with quartz at reservoir temperature (Simmons et al., 2025). Upon production to the surface, the silica-laden liquid will exceed amorphous silica saturation, which can result in silica deposition. The incorporation of deeply derived carbon dioxide into injected water permeating the reservoir causes weak acidification that reduces the mineral saturation indices of carbonate phases and impedes colloid growth of amorphous silica.

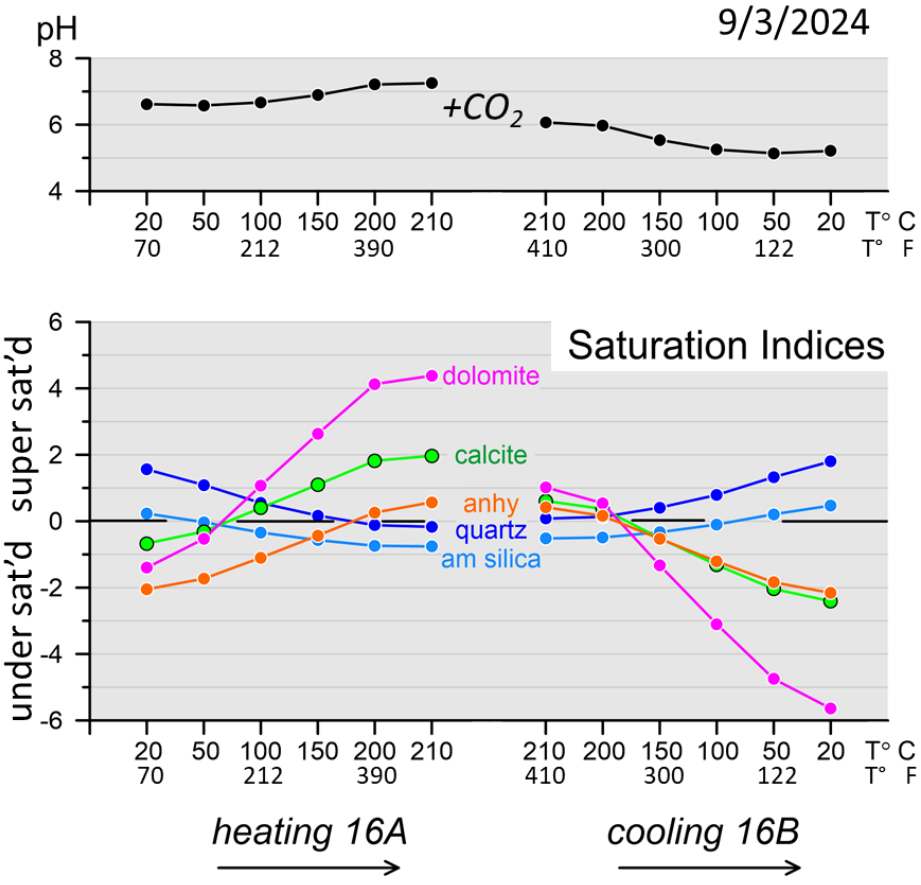

Figure 15: Summary of computed pH and saturation indices for quartz, amorphous silica, calcite, dolomite, and anhydrite as a function of temperature. Values above zero represent supersaturated waters, and values below zero represent undersaturated waters. These values were calculated using the Spec8 module in Geochemists Workbench utilizing geochemical data from injected and produced fluids collected on September 3, 2024 during a circulation experiment. These results indicate that carbonate minerals are prone to deposition in the well and in the reservoir upon injection and heating. By contrast, quartz and amorphous silica are prone to deposition in surface pipework and equipment due to cooling of produced waters.

5. WATER TREATMENT ADDITIVES

Antiscalants and corrosion inhibitors have been successfully utilized reducing scale and corrosion during site activities, including a circulation test lasting up to four weeks. The shift to longer-term circulation tests, beginning in 2026, will require close monitoring to ensure the dose rates and the mix of additives remain effective. The overarching goal is to achieve a steady state chemical condition that minimizes treatments (and therefore cost) while inhibiting scaling and corrosion detrimental to geothermal production.

To date an amino methylene phosphonic acid and a filming amine for carbon steel have been effective in inhibiting scale and corrosion, respectively. For upcoming, longer duration, circulation testing the following products are planned to be used: 1) a chelating agent to sequester Ca (and other metals) to prevent scaling; 2) a water-treatment polymer based on polyacrylic acid that acts as an anionic (negatively charged) polyelectrolyte that stabilizes microcrystals in solution so they don't deposit while also dispersing colloidal silica by interfering with silica polymerization; and as before 3) a filming amine for carbon steel protection. In addition to the scale inhibiters being introduced, the pH reduction due to the influx of reservoir CO_2 will aid in reducing mineral deposition.

6. CONCLUSIONS

1. Calcite is the dominant scale mineral across all samples, with less abundant siderite, anhydrite, halite, sylvite, and an expandable Si and Fe-rich smectitic clay.

2. Corrosion products reflect substrate composition, with magnetite, hematite, lepidocrocite and goethite forming on Fe-bearing components, and boehmite and an Al-rich phase with structural similarity to greenalite forming on aluminum components.

3. Proppant dissolution and clay mineral deposition demonstrate active water-rock interaction during long-term residence in the reservoir.

4. Dissolution of anhydrite within the recovered proppant suggests oscillating P-T-X conditions.

5. The injected fluids contain significant Ca and Mg. On heating to temperatures in excess of ~60°C carbonates and anhydrite are expected to precipitate.

6. The injected fluids rapidly equilibrate with quartz in the subsurface at reservoir temperatures, and the dissolved silica has the potential to deposit amorphous and/or quartz on cooling; however, no evidence of silica deposition has been observed thus far.

7. The incorporation of CO_2 into the circulating fluids within the reservoir imparts a weak acidification, partially mitigating carbonate and silica deposition.

8. The low abundances of calcite and anhydrite in recovered proppant suggest effective scale inhibitor performance.

9. Continued monitoring and adaptive water chemistry management are essential for sustaining EGS performance.

7. ACKNOWLEDGMENTS

This work was supported by the Office of Geothermal and the U.S. Department of Energy under project DE-EE0007080

8. REFERENCES

Jones, C., Simmons, S., & Moore, J. (2024). Geology of the Utah Frontier Observatory for Research in Geothermal Energy (FORGE) Enhanced Geothermal System (EGS) Site. Geothermics, 122, 103054.2024

Jones, C. G., England, K., Simmons, S., Rose, P., Mella, M., Barker, B., McLennan, J and Moore, J. (2023). Stimulation, Tracers and Geochemistry at Utah FORGE. In., Proceedings, Forty-Eighth Workshop on Geothermal Reservoir Engineering. Stanford University.

Simmons, S., Jones, C., Rose, P., Moore, J., (2025). The Geochemistry of Flowback and Produced Waters at Utah FORGE and Their Implications for EDS production. In., Proceedings, 50th Workshop on Geothermal Reservoir Engineering. Stanford California.

Moore, D. M. and R. C. Reynolds Jr. (1997) X-ray Diffraction and the Identification and Analysis of Clay Minerals. Oxford University Press, New York, New York. 378 p.